Electroweak radiative corrections to polarized top quark pair production

A. Arbuzov and S. Bondarenko*
Bogoliubov Laboratory of Theoretical Physics, JINR, 141980 Dubna, Moscow region, Russia

L. Kalinovskaya, R. Sadykov, and V. Yermolchyk†
Dzhelepov Laboratory of Nuclear Problems, JINR, 141980 Dubna, Moscow region, Russia

(Received 16 May 2023; accepted 8 June 2023; published 30 June 2023)

Electroweak effects in the $e^+e^- \to t\bar{t}$ annihilation process are described by taking into account polarization of the initial and final particles. We investigate the effects of complete one-loop electroweak radiative corrections (RCs) and higher-order radiative effects to the total cross section and analyze different types of asymmetries for polarized initial and final states for typical energies and degrees of polarization of the ILC and CLIC projects. Numerical results are obtained with the help of Monte Carlo tools: the `ReneSANCe` event generator and the `MCSANC` integrator.

DOI: 10.1103/PhysRevD.107.113006

I. INTRODUCTION

At a future high-energy e^+e^- collider, top quarks will be primarily produced via the electroweak annihilation process $e^+e^- \to \gamma, Z \to t\bar{t}$. The mass of the top quark can then be directly measured with a high precision unreachable at hadron colliders. Looking for effects of new physics in interactions of top quarks is also a very attractive and valuable objective for future experiments. Thus, having accurate predictions for various observables for processes involving top quarks is crucial, both for tests of the Standard Model and for new physics searches.

The physical programs for experiments with polarized e^+ and e^- beams at ILC [1–3] and CLIC [4] suggest measurement of not only the total cross section for $t\bar{t}$ production but also the different types of asymmetries. Both the photon and Z boson couplings of the top quark can be unambiguously measured using these observables [5].

In addition to ILC and CLIC, a scenario of longitudinally polarized colliding beams for the CEPC is considered [6]. In particular, these arguments suggest that polarization should be taken into account in the corresponding theoretical support and Monte Carlo codes.

Recently the study for the expected precision of the top quark mass and width in $t\bar{t}$ production using an energy scan around the threshold based on the CEPC scenario, assuming a total integrated luminosity of 100 fb^{-1}, shows that CEPC is capable of measuring the top quark mass with a precision below 34 MeV [7]. This study is performed with the help of the `QQbar_threshold` package [8].

The theoretical uncertainty for observables of top quark pair production at the one-loop level $\mathcal{O}(\alpha)$ were estimated for the first time in [9] for the unpolarized case and in [10,11] for different beam polarizations. Those studies were carried out using the Grace-Loop system [12,13].

Within the SANC project we have a library for electroweak (EW) building blocks (self-energies, vertices, boxes) in the unitary and R_ξ gauges for the process $e^+e^- \to t\bar{t}$ at the one-loop level [14,15]. We use spin and helicity analysis in combination with the spinor-helicity formalism to calculate the helicity amplitudes of the one-loop cross section components [16].

In this paper we consider theoretical uncertainties associated with electroweak and higher-order effects taking into account polarization of the initial and final particles for the processes of electron-positron annihilation into a top-quark pair

$$e^+(p_1,\chi_1) + e^-(p_2,\chi_2) \to \\ \to t(p_3,\chi_3) + \bar{t}(p_4,\chi_4)(+\gamma(p_5,\chi_5)), \qquad (1)$$

with arbitrary particle helicities χ_i. The main goal of this work is to calculate and study three main types of observables in this process; the total and differential cross section σ_t, several top-quark asymmetries, and polarization P_t of the final top quark. We take a close look at the size of various sources of EW radiation corrections and carefully examine the QED initial state radiation (ISR) effects.

We consider the beam energies that correspond to the experimental programs of the top quark property studies.

*bondarenko@jinr.ru
†Also at Institute for Nuclear Problems, Belarusian State University, Minsk 220006, Belarus.

First, at the production threshold, e.g., at 350 GeV center-of-mass energy, the top-quark mass can be measured with a high precision hopefully below 0.1%. Second, at 500 GeV center-of-mass energy it is convenient to measure weak and electromagnetic couplings of the top quark. This energy region also provides an excellent sensitivity to the effect of physics beyond the Standard Model [17–19].

QCD radiative corrections to the process of top-quark pair production have been extensively studied both at the threshold energy where resummation of higher-order effects is important [20–22] and above it within pertubative QCD [23,24]. The next-to-next-to-leading-order (NNLO) QCD corrections were also calculated for unpolarized and polarized cross sections and forward-backward asymmetries in this process [25–28]. In [29] NNLO electroweak corrections were considered together with QCD effects at the threshold. Recently, next-to-leading-order (NLO) QCD corrections have also been presented for the process with subsequent decays of the produced (off shell) top quarks into bottom quarks and W bosons [30]. We will no more discuss QCD effects in this paper, leaving the question about their interplay with EW effects for further studies.

The article is organized as follows. The next section contains preliminary remarks and the general notations. In Sec. III we present the numerical results and a comprehensive comparison of independent Monte Carlo codes for cross-checking and the evaluation of theoretical uncertainties for observables for polarized and unpolarized cases. The last section contains a discussion and conclusions.

II. RADIATIVE CORRECTIONS TO TOP QUARK PAIR PRODUCTION IN SANC

We presented a detailed review of the techniques and results of the analytic calculations of the NLO EW scalar form factors and helicity amplitudes of the general $e^+e^- \to f\bar{f}$ in our paper on the s-channel lepton-pair production [16] (note the additional color factor in the final state).

We evaluate the Born level leading-order (LO) cross section σ^{Born} contribution with both photon and Z-boson exchange.

Gauge invariant subsets of one-loop QED corrections are evaluated separately, i.e., the initial state radiation, the final-state radiation (FSR), and the initial-final interference (IFI).

We define the pure weak contribution as the difference between the complete one-loop electroweak correction and the pure QED part of it. The corresponding relative contributions of the weak and leading higher-order corrections will be further denoted as δ^{weak} and δ^{ho}, respectively. The complete one-loop δ^{weak} consists of pure weak interaction and vacuum polarization (VP) contributions.

We evaluate the leading higher-order EW corrections δ^{ho} to four-fermion processes through the $\Delta\alpha$ and $\Delta\rho$ parameters. A detailed description of our implementation of this contribution was presented in [31]. At two-loop level the above corrections consist of the EW at $\mathcal{O}(G_\mu^2)$ and the mixed EW $\otimes$ QCD at $\mathcal{O}(G_\mu\alpha_s)$ parts.

Thus the total EW cross section can be presented as

$$\sigma = \sigma^{\mathrm{Born}} + \sigma^{\mathrm{QED}} + \sigma^{\mathrm{weak}} + \sigma^{\mathrm{ho}}. \tag{2}$$

Additionally we estimate the multiple-photon initial-state radiation corrections. The implementation in SANC of these type of corrections in the leading logarithmic approximation (LLA) through the approach of QED structure functions [32,33] was described in detail in [34]. The results are shown up to $\mathcal{O}(\alpha^3 L^3)$ finite terms for the exponentiated representation and up to $\mathcal{O}(\alpha^4 L^4)$ for the order-by-order calculations. The corresponding relative corrections are denoted below as $\delta^{\mathrm{LLA,ISR}}$. The master formula for a general e^+e^- annihilation cross section with ISR QED corrections in the leading logarithmic approximation has the same structure as the one for the Drell-Yan process. For ISR corrections in the annihilation channel, the large logarithm is $L = \ln(s/m_e^2)$, where the total center-of-mass energy $\sqrt{s}$ is chosen as a factorization scale. In the LLA approximation, we separate the pure photonic corrections (marked "γ") and the remaining ones, which include the pure pair and mixed photon-pair effects (marked "e^+e^-" or "$\mu^+\mu^-$").

The complete two-loop corrections due to initial state radiation for the unpolarized process $e^+e^- \to \gamma^*, Z$ were first calculated in [35]. Those results were verified and partially corrected in [36]. Leading and next-to-leading multiple photon initial state radiation corrections were computed within the QED structure function formalism in [37] up to the $\mathcal{O}(\alpha^6 L^5)$ order, where $L = \ln s/m_e^2$ is the so-called large logarithm.

III. NUMERICAL RESULTS AND COMPARISONS

Numerical results for the polarized top quark pair production contain estimates of the total cross sections, as well as energy/angular distributions, various polarization effects and the study of different types of asymmetries for polarized initial and final states.

Here we used the following set of input parameters:

$$\begin{aligned}
&\alpha^{-1}(0) = 137.035999084, \qquad g = 1.1663787 \times 10^{-5},\\
&M_W = 80.379\ \mathrm{GeV}, \qquad M_Z = 91.1876\ \mathrm{GeV},\\
&M_H = 125\ \mathrm{GeV}, \qquad m_e = 0.51099895\ \mathrm{MeV},\\
&m_\mu = 0.1056583745\ \mathrm{GeV}, \qquad m_\tau = 1.77686\ \mathrm{GeV},\\
&m_d = 0.083\ \mathrm{GeV}, \qquad m_s = 0.215\ \mathrm{GeV},\\
&m_b = 4.7\ \mathrm{GeV}, \qquad m_u = 0.062\ \mathrm{GeV},\\
&m_c = 1.5\ \mathrm{GeV}, \qquad m_t = 172.76\ \mathrm{GeV}.
\end{aligned} \tag{3}$$

The following angular cuts are applied:

$$|\cos\vartheta_t| < 0.9, \qquad |\cos\vartheta_{\bar{t}}| < 0.9, \tag{4}$$

TABLE I. The tuned triple comparison of the hard photon bremsstrahlung cross section σ^{hard} (pb) between SANC (S), CalcHEP (C), and WHIZARD (W).

P_{e^+}, P_{e^-}	0,0	$+1,-1$	$-1,+1$
	$\sqrt{s} = 350$ GeV		
S	0.13284(1)	0.38126(1)	0.15013(1)
W	0.13282(2)	0.38120(1)	0.15021(5)
C	0.13285(1)	0.38124(4)	0.15014(1)
	$\sqrt{s} = 500$ GeV		
S	0.46733(1)	1.3090(1)	0.55987(2)
W	0.46730(2)	1.3093(4)	0.55989(4)
C	0.46728(3)	1.3088(1)	0.55983(5)

where ϑ_t and $\vartheta_{\bar{t}}$ are the angles with respect to the electron beam axis.

The results are obtained for the center-of-mass energies $\sqrt{s} = 350$ GeV and 500 GeV and for unpolarized $(P_{e^+}, P_{e^-}) = (0, 0)$, fully $(P_{e^+}, P_{e^-}) = (+1, -1), (-1, +1)$ and partially $(P_{e^+}, P_{e^-}) = (-0.3, 0.8), (0.3, -0.8), (0, 0.8)$, $(0, -0.8)$ polarized positron/electron beams.

Most calculations are done in the $\alpha(0)$ EW scheme in order to have direct access to the effect of vacuum polarization. In this scheme, the fine structure constant $\alpha(0)$ and all particle masses are input parameters. Additional investigations are performed for scheme dependencies between $\alpha(0)$ and G_μ EW schemes.

A. Comparison with other codes

We calculated polarized cross sections at the tree level for the Born and hard photon bremsstrahlung and compared them with the results of the CalcHEP [38] and WHIZARD [39,40] codes. The Born results agree in all digits for all three codes, and therefore the corresponding table is omitted.

The comparison of the hard bremsstrahlung results is shown in Table I. The calculations are done in the $\alpha(0)$ EW scheme with fixed 100% polarized initial states for $\sqrt{s} =$ 350 GeV and 500 GeV, angular cuts (4), and an additional cut on the photon energy $E_\gamma \geq 10^{-4}\sqrt{s}/2$. The table shows results for the unpolarized and fully polarized components $(+1,-1)$, $(-1,+1)$, while results for the components $(+1,+1)$, $(-1,-1)$ are of a different (smaller) order of magnitude, i.e., $1.8(1) \times 10^{-7}$ pb for $\sqrt{s} = 350$ GeV and $0.238(1) \times 10^{-3}$ pb for $\sqrt{s} = 500$ GeV for all codes. A very good agreement within statistical errors with the above-mentioned codes is found.

A comprehensive comparison has been made for complete one-loop electroweak radiative corrections obtained with our codes (ZFITTER and SANC) [14,41] as well as with the results of the topfit code [42,43]. We also compared the results of the NLO EW relative corrections calculations of the Grace-Loop code as a function of the energy for the unpolarized and polarized cases presented in [12,13]. The qualitative analysis shows a good agreement.

B. Total cross section

The corresponding results for the total cross section (2) are presented in Table II where the relative corrections δ^i are computed as the ratios (in percent) of the corresponding RC contributions to the Born-level cross section.

One-loop and higher-order weak-interaction corrections strongly depend on the choice of the EW scheme, and the total weak corrections in the G_μ scheme are smaller by about 5–6% than in the $\alpha(0)$ one.

The integrated cross sections for the weak and leading higher-order corrections in the $\alpha(0)$ and G_μ schemes and their relative difference

TABLE II. Integrated Born and one-loop cross sections and relative corrections for unpolarized and fully polarized initial beams at the center-of-mass energies $\sqrt{s} = 350$ GeV and 500 GeV.

P_{e^+}, P_{e^-}	0, 0	$+1, -1$	$-1, +1$	$0.3, -0.8$	$-0.3, 0.8$	$0, -0.8$	0, 0.8
				$\sqrt{s} = 350$ GeV			
σ^{Born}, pb	0.22431(1)	0.64367(1)	0.25357(1)	0.38542(1)	0.17086(1)	0.30232(1)	0.14629(1)
σ^{NLO}, pb	0.16623(1)	0.45972(1)	0.20520(1)	0.27612(1)	0.13612(1)	0.21713(1)	0.11532(1)
δ^{NLO}, %	−25.90(1)	−28.58(1)	−19.07(1)	−28.36(1)	−20.33(1)	−28.18(1)	−21.17(1)
δ^{QED}, %	−39.87(1)	−39.79(1)	−40.03(1)	−39.80(1)	−40.01(1)	−39.81(1)	−39.99(1)
δ^{VP}, %	12.84(1)	11.00(1)	17.51(1)	11.15(1)	16.65(1)	11.28(1)	16.08(1)
$\delta^{\text{weak−VP}}$, %	1.11(1)	0.20(1)	3.43(1)	0.27(1)	3.01(1)	0.33(1)	2.72(1)
δ^{ho}, %	1.50(1)	1.47(1)	1.55(1)	1.48(1)	1.54(1)	1.48(1)	1.53(1)
				$\sqrt{s} = 500$ GeV			
σ^{Born}, pb	0.45030(1)	1.2609(1)	0.54028(1)	0.75654(1)	0.36020(1)	0.59444(1)	0.30617(1)
σ^{NLO}, pb	0.45865(1)	1.2334(1)	0.60072(1)	0.74267(1)	0.39468(4)	0.58522(1)	0.33212(1)
δ^{NLO}, %	1.86(1)	−2.18(1)	11.12(1)	−1.83(1)	9.58(1)	−1.55(1)	8.48(1)
δ^{QED}, %	−4.08(1)	−3.91(1)	−4.56(1)	−3.92(1)	−4.46(1)	−3.91(1)	−4.40(1)
δ^{VP}, %	12.58(1)	10.97(1)	16.33(1)	11.11(1)	15.67(1)	11.22(1)	15.22(1)
$\delta^{\text{weak−VP}}$, %	−6.63(1)	−9.24(1)	−5.63(1)	−9.02(1)	−1.63(1)	−8.84(1)	−2.35(1)
δ^{ho}, %	1.73(1)	1.69(1)	1.82(1)	1.69(1)	1.80(1)	1.69(1)	1.79(1)

TABLE III. Integrated Born and weak contributions to the cross section and higher-order leading corrections in two EW schemes: $\alpha(0)$ and G_μ at the center-of-mass energies $\sqrt{s} = 350$ GeV and 500 GeV.

$\sqrt{s}$, GeV	350	500
$\sigma^{\rm Born}_{\alpha(0)}$, pb	0.22431(1)	0.45030(1)
$\sigma^{\rm Born}_{G_\mu}$, pb	0.24108(1)	0.48398(1)
$\delta^{\rm Born}_{G_\mu/\alpha(0)}$, %	7.48(1)	7.48(1)
$\sigma^{\rm weak}_{\alpha(0)}$, pb	0.25564(1)	0.47705(1)
$\sigma^{\rm weak}_{G_\mu}$, pb	0.26055(1)	0.48420(1)
$\delta^{\rm weak}_{G_\mu/\alpha(0)}$, %	1.92(1)	1.50(1)
$\sigma^{\rm weak+ho}_{\alpha(0)}$, pb	0.25900(1)	0.48483(1)
$\sigma^{\rm weak+ho}_{G_\mu}$, pb	0.25986(1)	0.48289(1)
$\delta^{\rm weak+ho}_{G_\mu/\alpha(0)}$, %	0.33(1)	−0.40(1)

$$\delta_{G_\mu/\alpha(0)} = \frac{\sigma_{G_\mu}}{\sigma_{\alpha(0)}} - 1, \% \tag{5}$$

are presented in Table III. Ratio (5) shows the stabilization of the results and can be considered as an estimation of the theoretical uncertainty of the weak and higher-order contributions. As is well known, the difference between two EW schemes in the LO is just the ratio of the EW couplings and gives $\delta^{\rm LO}_{G_\mu/\alpha(0)} = 7.5\%$. As is seen from the Tables, the weak contribution reduces the difference to about 2% at the energy of 350 GeV and 1.5% at 500 GeV. Moreover, the sum of the weak and higher-order contributions reduces the difference to about 0.33% at 350 GeV and −0.4% at 500 GeV.

C. Multiple photon ISR corrections in the LLA approximation

Here we discuss the estimation of the initial-state photon radiations in detail. In Table IV we show the corresponding results for the multiple photon ISR corrections of different order of $\mathcal{O}(\alpha^n L^n), n = 2$–4 in the LLA approximation for the center-of-mass energies $\sqrt{s} = 350$ GeV and 500 GeV in the $\alpha(0)$ EW scheme. The relative corrections δ^i are computed as the ratios (in percent) of the corresponding RC contributions to the Born-level cross section. The most significant contribution is of course the photonic one of the order $\mathcal{O}(\alpha L)^2$. For the center-of-mass energy $\sqrt{s} =$ 350 GeV, the dominant contributions of the second order are about +8.397% for γ and −0.460% for e^+e^--pairs (−0.277% for $\mu^+\mu^-$-pairs). Similar behavior occurs for the energy $\sqrt{s} = 500$ GeV, but orders of magnitudes of the multiple photon corrections are much smaller.

When considering multiple photon corrections, we see that it is certainly sufficient to take into account corrections up to the fourth order.

TABLE IV. Multiple photon ISR relative corrections δ (%) in the LLA approximation at $\sqrt{s} = 350$ GeV and 500 GeV with cuts (4).

$\sqrt{s}$, GeV	350	500
$\mathcal{O}(\alpha L)$, γ	−42.546(1)	−3.927(1)
$\mathcal{O}(\alpha^2 L^2)$, γ	+8.397(1)	−0.429(1)
$\mathcal{O}(\alpha^2 L^2)$, e^+e^-	−0.460(1)	−0.030(1)
$\mathcal{O}(\alpha^2 L^2)$, $\mu^+\mu^-$	−0.277(1)	−0.018(1)
$\mathcal{O}(\alpha^3 L^3)$, γ	−0.984(1)	+0.021(1)
$\mathcal{O}(\alpha^3 L^3)$, e^+e^-	+0.182(1)	−0.012(1)
$\mathcal{O}(\alpha^3 L^3)$, $\mu^+\mu^-$	+0.110(1)	−0.008(1)
$\mathcal{O}(\alpha^4 L^4)$, γ	+0.070(1)	+0.002(1)

D. Differential distributions

1. Angular distributions

In Figs. 1 and 2, the LO (dashed line) and NLO EW (solid line) cross sections (upper panel), as well as the relative corrections (lower panel) are shown. The left part of Fig. 1 corresponds to the unpolarized (black), and fully polarized, with $(P_{e^+}, P_{e^-}) = (+1, -1)$ (red) and $(-1, +1)$ (blue), initial beams, while the right one shows the partially polarized initial beams with $(P_{e^+}, P_{e^-}) = (+0.3, -0.8)$ (red) and $(-0.3, +0.8)$ (blue) for the energy $\sqrt{s} =$ 350 GeV. Figure 2 shows the same but for $\sqrt{s} = 500$ GeV.

The radiative corrections significantly reduce cross sections at the energy $\sqrt{s} = 350$ GeV in the whole range of the scattering angles. The corresponding relative corrections are large, negative and varied from −32% to −12% for unpolarized/fully polarized states. The real planned polarized states in the ILC experiment (right panel) show significant dependence on the polarization of the initial beams, namely, for $(P_{e^+}, P_{e^-}) = (+0.3, -0.8)$ the relative corrections are $-(25 - 32)\%$ while for $(-0.3, +0.8)$ they are $-(18 - 20)\%$.

At the center-of-mass energy $\sqrt{s} = 500$ GeV the LO and NLO EW differential cross sections can cross each other and therefore the relative corrections can change the sign. The dependence on polarization is also strong, and δ are from 15% to −10% for $(+0.3, -0.8)$ and from 20% to 0% for $(-0.3, +0.8)$.

It should also be noted that the nonphysical dips in the first and last bins of the relative correction histograms are due to the angular limits (4) and can be removed by applying wider cuts.

2. Energy dependence

In Fig. 3 the unpolarized cross sections for the LO and for NLO EW in parts are presented. The upper panel shows the cross sections for the QED and weak gauge-invariant contributions to NLO EW while the lower panel demonstrates the corresponding relative corrections to the Born cross section subdivided inside the QED (ISR, IFI, FSR)

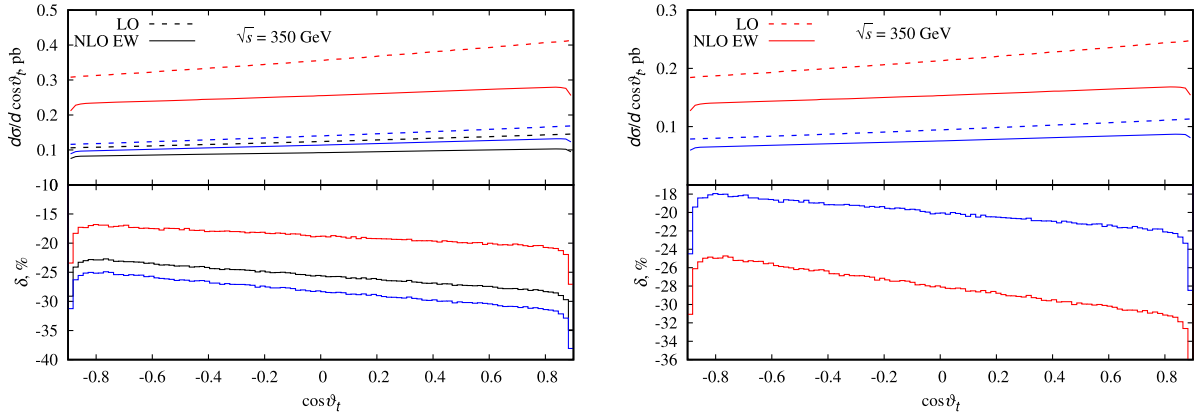

FIG. 1. LO and EW NLO cross sections and relative corrections at $\sqrt{s} = 350$ GeV with (un)polarized initial beams.

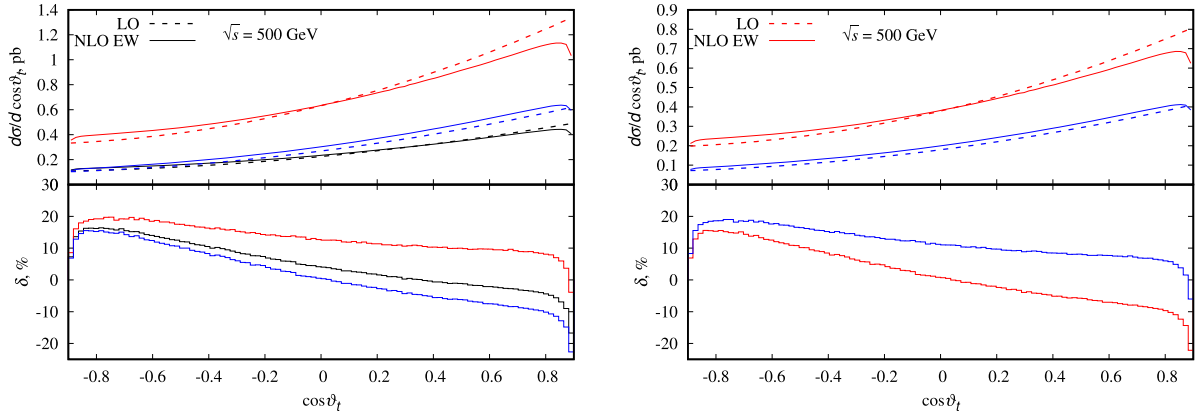

FIG. 2. The same as in Fig. 1 but for $\sqrt{s} = 500$ GeV.

and weak (VP and weak-VP) sectors. The contributions of the leading higher-order corrections are present as well.

It is seen from the figure that the total NLO EW contribution near the threshold at the center-of-mass energy $\sqrt{s} = 350$ GeV is defined by large negative QED (about −35%) and positive weak (15%) contributions, then at approximately $\sqrt{s} = 450$ GeV they compensate each other, and above that energy QED part dominates. It should be noted that in the QED contribution the ISR part dominates while in the weak contribution the VP part dominates. The leading higher-order two-loop contributions are rather low, about 1.5–2%, but play an important role in the EW scheme-dependency stabilization.

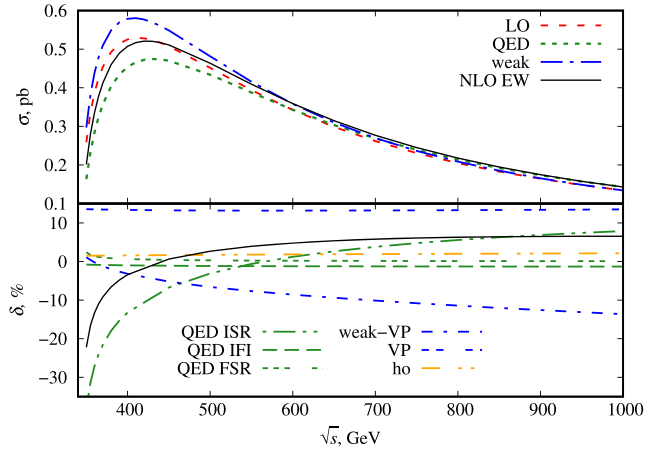

FIG. 3. The LO and NLO EW corrected unpolarized cross sections and the relative corrections in parts as a function of the center-of-mass energy.

E. Asymmetries

In this section we analyze the effect of radiative corrections for different types of asymmetries: the left-right A_{LR} and forward-backward A_{FB} asymmetries, as well as the final-state quark polarization P_t.

1. Left-right asymmetry A_{LR}

The asymmetry A_{LR} is defined in the following form:

$$A_{\mathrm{LR}} = \frac{\sigma_{\mathrm{LR}} - \sigma_{\mathrm{RL}}}{\sigma_{\mathrm{LR}} + \sigma_{\mathrm{RL}}},$$

where σ_{LR} and σ_{RL} are the cross sections for the fully polarized electron-positron $e^-_{\mathrm{L}}e^+_{\mathrm{R}}$ and $e^-_{\mathrm{R}}e^+_{\mathrm{L}}$ initial states, respectively. For the given definition, A_{LR} does not depend

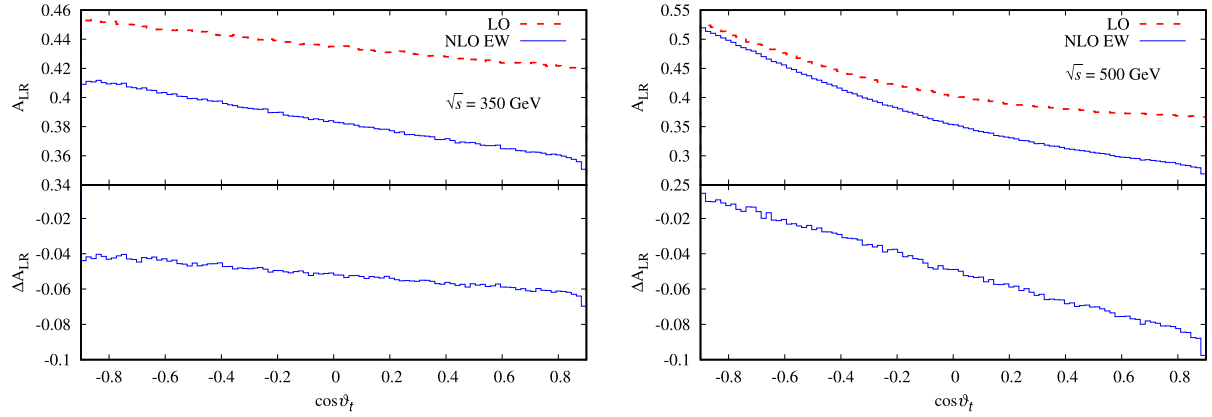

FIG. 4. The asymmetry A_{LR} in the Born and one-loop approximations at $\sqrt{s} = 350$ GeV (left) and $\sqrt{s} = 500$ GeV (right) vs the cosine of the scattering angle.

on the degrees of the initial beam polarization, but this type of asymmetry is sensitive to electroweak interaction effects.

In Fig. 4, the left-right asymmetry distributions for the Born and one-loop contributions are shown as a function of the cosine of the top-quark scattering angle. The corresponding shift of the asymmetry

$$\Delta A_{\mathrm{LR}} = A_{\mathrm{LR}}(\mathrm{NLO\ EW}) - A_{\mathrm{LR}}(\mathrm{LO})$$

is shown in the lower panel.

At the center-of-mass energy $\sqrt{s} = 350$ GeV ΔA_{LR} changes from about -0.04 to -0.06 while at $\sqrt{s} =$ 500 GeV it changes from about -0.01 to -0.09 over the whole range of the top-quark scattering angles.

2. *Forward-backward asymmetry* A_{FB}

The forward-backward asymmetry is defined as

$$A_{\mathrm{FB}} = \frac{\sigma_{\mathrm{F}} - \sigma_{\mathrm{B}}}{\sigma_{\mathrm{F}} + \sigma_{\mathrm{B}}},$$

where

$$\sigma_{\mathrm{F}} = \int_0^1 \frac{d\sigma}{d\cos\vartheta_t} d\cos\vartheta_t, \qquad \sigma_{\mathrm{B}} = \int_{-1}^0 \frac{d\sigma}{d\cos\vartheta_t} d\cos\vartheta_f.$$

In Fig. 5, the asymmetry A_{FB} in the Born (dashed) and one-loop (solid) approximations (upper panel) and the corresponding shift

$$\Delta A_{\mathrm{FB}} = A_{\mathrm{FB}}(\mathrm{NLO\ EW}) - A_{\mathrm{FB}}(\mathrm{LO})$$

(lower panel) as a function of $\sqrt{s}$ are presented. On the left, the black lines are for the unpolarized initial beams while the red and blue ones are for the fully polarized cases $(P_{e^+}, P_{e^-}) = (+1, -1)$ and $(-1, +1)$, respectively. On the right, the red and blue lines are for the partially polarized beams with $(P_{e^+}, P_{e^-}) = (+0.3, -0.8)$ and $(-0.3, +0.8)$, respectively.

One can see that a combination of degrees of initial particles polarization can either decrease $(P_{e^+}, P_{e^-}) = (+0.3, -0.8)$ or increase $(P_{e^+}, P_{e^-}) = (-0.3, -0.8)$ the A_{FB} asymmetry with respect to the unpolarized case.

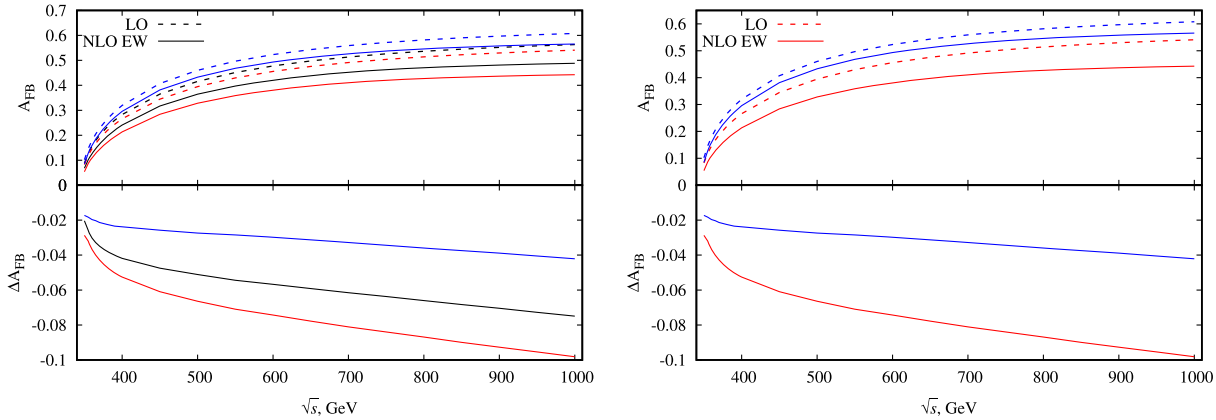

FIG. 5. The asymmetry A_{FB} in the Born and one-loop approximations and the corresponding shift as a function of the center-of-mass energy. Details are in the text.

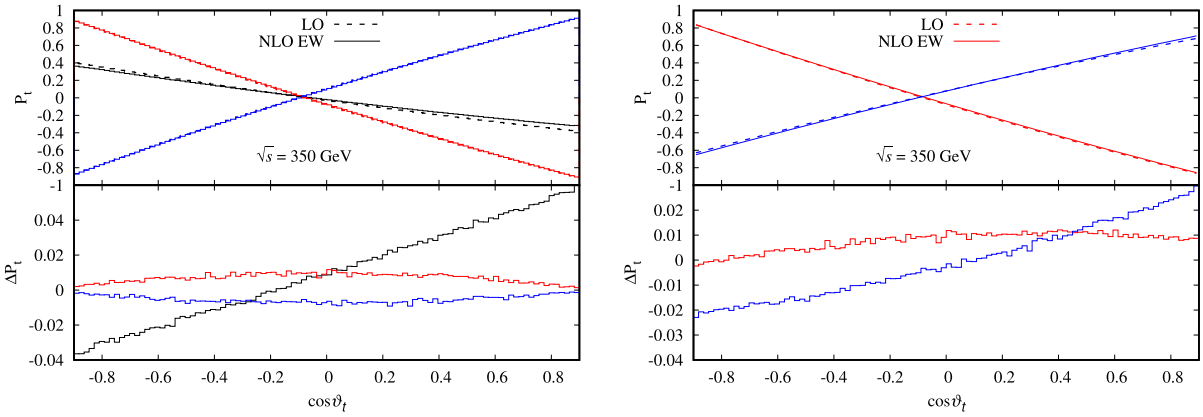

FIG. 6. Top-quark polarization P_t in the Born and one-loop approximations and the corresponding shifts ΔP_t vs the scattering angle at the center-of-mass energy $\sqrt{s} = 350$ GeV. Details are in the text.

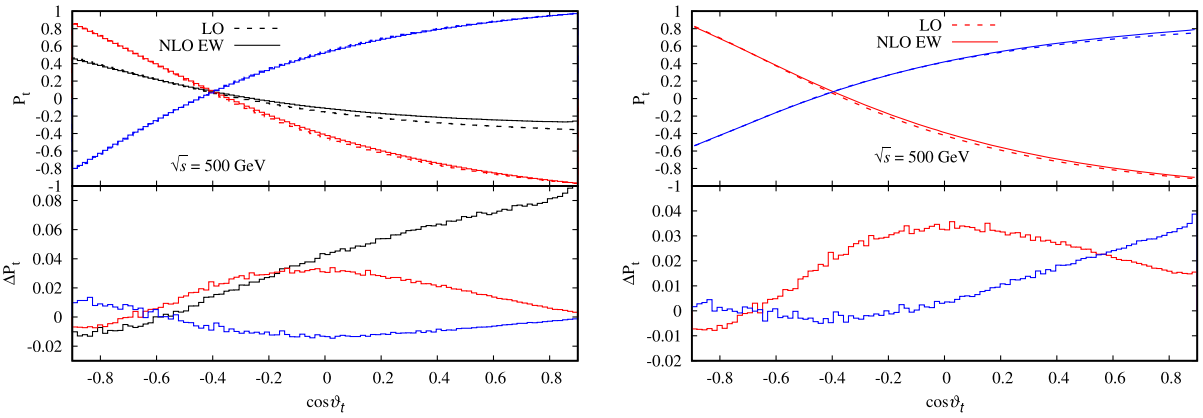

FIG. 7. The same as in Fig. 6 but for $\sqrt{s} = 500$ GeV.

The asymmetry A_{FB} is zero both for LO and NLO EW at the threshold and increase with increasing energy. The NLO EW corrections decrease the LO results, and ΔA_{FB} is always negative in the c.m.s energy range $\sqrt{s} = 350$–1000 GeV.

3. *Final-state fermion polarization P_t*

The polarization of a final-state top quark P_t can be expressed as the ratio between the difference of the cross sections for the right- and left-handed final state helicities and their sum

$$P_t = \frac{\sigma_{\mathrm{R}_t} - \sigma_{\mathrm{L}_t}}{\sigma_{\mathrm{R}_t} + \sigma_{\mathrm{L}_t}}.$$

In Figs. 6 and (7), the top quark polarization in the Born (dashed) and one-loop (solid) approximations (upper panel) and the corresponding shift (lower panel)

$$\Delta P_t = P_t(\mathrm{NLO\ EW}) - P_t(\mathrm{LO})$$

at the center-of-mass energy $\sqrt{s} = 350$ (500) GeV. On the left, the black lines are for the unpolarized initial beams while the red and blue ones are for the fully polarized cases of $(P_{e^+}, P_{e^-}) = (+1, -1)$ and $(-1, +1)$, respectively. On the right, the red and blue lines are for partially polarized beams with $(P_{e^+}, P_{e^-}) = (+0.3, -0.8)$ and $(-0.3, +0.8)$, respectively.

This asymmetry is important for studying possible manifestations of CP violation beyond the Standard Model [44].

The results for P_{t} are very much affected by initial-beam polarizations. The difference ΔP_t also depends on the center-of-mass energy and initial-beam polarizations. The largest values of ΔP_t for unpolarized initial beams are -0.04 to 0.05 at $\sqrt{s} = 350$ GeV and -0.01 to 0.08 at 500 GeV. Polarization of the initial states significantly reduces ΔP_t both at 350 GeV and 500 GeV.

IV. CONCLUSION

In this paper, we investigated electroweak corrections to the process of electron-positron annihilation into a top-quark pair with allowance for polarizations of the initial and final particles. Numerical results are presented for energies

and polarizations which are typical of the future CLIC and ILC linear e^+e^- collider projects.

The calculated polarized cross sections at the tree level for the Born and hard photon bremsstrahlung were thoroughly compared with the CalcHEP and WHIZARD results. A very good agreement was observed.

Then virtual (loop) EW corrections were calculated within the SANC system. Numerical studies were carried out for several observables in the $t\bar{t}$ production process for unpolarized and polarized beams with taking into account the NLO EW level, higher-order corrections, and multiple photon ISR corrections.

We considered a set of benchmark polarizations and found that the relative effects of $e^{\pm}$ polarizations on the EW radiative correction are quite sizeable. In other words, one can not use the same correction factors for the cases of different degrees of beam polarization. The NLO EW corrections qualitatively agreed with the Grace-Loop results.

Various asymmetries which can be measured in the given process were analyzed. For all the asymmetries, the NLO EW effects are found to be quite sizable. The magnitude of EW radiative corrections to asymmetries at 500 GeV center-of-mass energy is higher than at 350 GeV in most cases.

It was demonstrated that a considerable EW scheme dependence still remains when the complete one-loop corrections are supplemented by the leading higher-order corrections. To reduce the corresponding uncertainty, we need complete two-loop EW radiative corrections for the process under consideration.

The numerical results presented here were obtained using the Monte Carlo generator `ReneSANCe` [45] and the `MCSANC` integrator which allow one to evaluate of arbitrary differential cross sections and to separate particular contributions.

ACKNOWLEDGMENTS

The research was supported by the Russian Science Foundation, Project No. 22-12-00021.

[1] ILC Collaboration, arXiv:1306.6352.
[2] K. Fujii *et al.*, arXiv:1506.05992.
[3] H. Aihara *et al.* (ILC Collaboration), arXiv:1901.09829.
[4] H. Abramowicz *et al.* (CLICdp Collaboration), J. High Energy Phys. 11 (2019) 003.
[5] C. Englert and M. Russell, Eur. Phys. J. C **77**, 535 (2017).
[6] Z. Duan, T. Chen, J. Gao, D. Ji, X. Li, D. Wang, J. Wang, Y. Wang, and W. Xia, JACoW **eeFACT2022** (2023), 97.
[7] Z. Li, X. Sun, Y. Fang, G. Li, S. Xin, S. Wang, Y. Wang, Y. Zhang, H. Zhang, and Z. Liang, Eur. Phys. J. C **83**, 269 (2023).
[8] M. Beneke, Y. Kiyo, A. Maier, and J. Piclum, Comput. Phys. Commun. **209**, 96 (2016).
[9] J. Fujimoto and Y. Shimizu, Mod. Phys. Lett. A **03**, 581 (1988).
[10] P. H. Khiem, E. Kou, Y. Kurihara, and F. Le Diberder, arXiv:1503.04247.
[11] N. M. U. Quach, Y. Kurihara, K. H. Phan, and T. Ueda, Eur. Phys. J. C **78**, 422 (2018).
[12] G. Belanger, F. Boudjema, J. Fujimoto, T. Ishikawa, T. Kaneko, K. Kato, and Y. Shimizu, Phys. Rep. **430**, 117 (2006).
[13] F. Yuasa *et al.*, Prog. Theor. Phys. Suppl. **138**, 18 (2000).
[14] A. Andonov, D. Bardin, S. Bondarenko, P. Christova, L. Kalinovskaya, and G. Nanava, arXiv:hep-ph/0202112.
[15] A. Andonov, D. Bardin, S. Bondarenko, P. Christova, L. Kalinovskaya, and G. Nanava, Phys. Part. Nucl. **34**, 577 (2003).
[16] S. Bondarenko, Y. Dydyshka, L. Kalinovskaya, R. Sadykov, and V. Yermolchyk, Phys. Rev. D **102**, 033004 (2020).
[17] E. Devetak, A. Nomerotski, and M. Peskin, Phys. Rev. D **84**, 034029 (2011).
[18] M. S. Amjad, M. Boronat, T. Frisson, I. Garcia, R. Poschl, E. Ros, F. Richard, J. Rouene, P. R. Femenia, and M. Vos, arXiv:1307.8102.
[19] M. S. Amjad *et al.*, Eur. Phys. J. C **75**, 512 (2015).
[20] A. H. Hoang, C. J. Reisser, and P. Ruiz-Femenia, Phys. Rev. D **82**, 014005 (2010).
[21] A. H. Hoang and M. Stahlhofen, J. High Energy Phys. 05 (2014) 121.
[22] M. Beneke, Y. Kiyo, P. Marquard, A. Penin, J. Piclum, and M. Steinhauser, Phys. Rev. Lett. **115**, 192001 (2015).
[23] Y. Kiyo, A. Maier, P. Maierhofer, and P. Marquard, Nucl. Phys. **B823**, 269 (2009).
[24] J. Gao and H. X. Zhu, Phys. Rev. D **90**, 114022 (2014).
[25] J. Gao and H. X. Zhu, Phys. Rev. Lett. **113**, 262001 (2014).
[26] L. Chen, O. Dekkers, D. Heisler, W. Bernreuther, and Z.-G. Si, J. High Energy Phys. 12 (2016) 098.
[27] W. Bernreuther, L. Chen, P.-C. Lu, and Z.-G. Si, J. High Energy Phys. 05 (2023) 094.
[28] J. G. Korner, A. Pilaftsis, and M. M. Tung, Z. Phys. C **63**, 575 (1994).
[29] M. Beneke, A. Maier, T. Rauh, and P. Ruiz-Femenia, J. High Energy Phys. 02 (2018) 125.
[30] A. Denner, M. Pellen, and G. Pelliccioli, Eur. Phys. J. C **83**, 353 (2023).
[31] A. B. Arbuzov, S. G. Bondarenko, L. V. Kalinovskaya, L. A. Rumyantsev, and V. L. Yermolchyk, Phys. Rev. D **105**, 033009 (2022).
[32] E. A. Kuraev and V. S. Fadin, Sov. J. Nucl. Phys. **41**, 466 (1985).

[33] O. Nicrosini and L. Trentadue, Phys. Lett. B **196**, 551 (1987).
[34] A. Arbuzov, S. Bondarenko, L. Kalinovskaya, R. Sadykov, and V. Yermolchyk, Symmetry **13**, 1256 (2021).
[35] F. A. Berends, W. L. van Neerven, and G. J. H. Burgers, Nucl. Phys. **B297**, 429 (1988); **B304**, 921(E) (1988).
[36] J. Blumlein, A. De Freitas, and W. van Neerven, Nucl. Phys. **B855**, 508 (2012).
[37] J. Blümlein and K. Schönwald, Mod. Phys. Lett. A **37**, 2230004 (2022).
[38] A. Belyaev, N. D. Christensen, and A. Pukhov, Comput. Phys. Commun. **184**, 1729 (2013).
[39] W. Kilian, T. Ohl, and J. Reuter, Eur. Phys. J. C **71**, 1742 (2011).
[40] M. Moretti, T. Ohl, J. Reuter, and O'Mega, An Optimizing matrix element generator, LC-TOOL-2001-040-rev, arXiv: hep-ph/0102195.
[41] D. Y. Bardin, L. Kalinovskaya, and G. Nanava, arXiv: hep-ph/0012080.
[42] J. Fleischer, J. Fujimoto, T. Ishikawa, A. Leike, T. Riemann, Y. Shimizu, and A. Werthenbach in *Proceedings of the Workshop on Computer Particle Physics: (CPP 2001): Automatic Calculation for Future Colliders* (2002), Vol. 3, pp. 153–162, arXiv:hep-ph/0203220.
[43] J. Fleischer, A. Leike, T. Riemann, and A. Werthenbach, Eur. Phys. J. C **31**, 37 (2003).
[44] G. A. Ladinsky and C. P. Yuan, Phys. Rev. D **49**, 4415 (1994).
[45] R. Sadykov, A. Arbuzov, S. Bondarenko, Y. Dydyshka, L. Kalinovskaya, L. Rumyantsev, and V. Yermolchyk, J. Phys. Conf. Ser. **2438**, 012152 (2023).